Uniform Wavelength Spacing Mach–Zehnder Interferometer Using Phase-Generating Couplers

Takayuki Mizuno, *Member, IEEE*, Tsutomu Kitoh, *Member, IEEE*, Manabu Oguma, Yasuyuki Inoue, *Member, IEEE*, Tomohiro Shibata, and Hiroshi Takahashi, *Member, IEEE*

***Abstract*—A theoretical and experimental study of an optical interferometer circuit with a uniform wavelength spacing is presented. The operating principle of the filter and a phase-generating coupler (PGC) that can transform a conventional filter into a uniform-wavelength-spaced optical filter is described. As an example, a transformation method is applied to a conventional Mach–Zehnder interferometer (MZI), and the PGC variables are optimized to obtain an MZI with a constant channel spacing of 20 nm. Furthermore, the designed MZI is fabricated using 1.5%-Δ silica-based planar lightwave circuit technology and a 20-nm-spaced MZI is realized with a wavelength displacement that was less than $\pm 1.2\%$ of the wavelength period. The fabrication tolerance of the MZI in relation to the PGC design variables is discussed. It is shown that a certain PGC design can increase the fabrication tolerance.**

***Index Terms*—Lattice filters, optical couplers, optical delay lines, optical filters, optical planar waveguides.**

I. Introduction

OPTICAL interferometer circuits composed of optical couplers and optical delay parts are a basic element employed in various optical devices [1]–[3]. Such circuits include Mach–Zehnder interferometers (MZIs) [4], lattice-form filters (or cascaded MZIs) [5], transversal-form filters [6], and interferometers with ring resonator filters [7]. These optical interferometer circuits have a periodic spectral response with respect to optical frequency, whose frequency period is inversely proportional to the unit delay [8]. Practical optical devices including optical add–drop multiplexers [9], frequency channel selectors [10], and interleave filters [11] have been proposed and developed. They are suitable for use with optical systems such as a dense wavelength-division multiplexing (DWDM) system, where the channel allocation is equally spaced with respect to optical frequency because these circuits have a periodic spectral response in terms of frequency.

Currently, new systems are being developed, where the channel allocation is equally spaced with respect to wavelength. One such system is the coarse wavelength-division multiplexing (CWDM) system whose main objective is to increase the transmission capacity of access/metro networks at low cost. The CWDM system allocates the wavelength grid with a 20-nm spacing usually with eight channels in the range of 1470–1610 nm. Various optical signal processing devices are essential if we are to implement such wavelength-based optical systems. MZI-based optical interferometer circuits are suitable for such applications because they can realize arbitrary transmission shapes within an FSR, e.g., a flat passband with a low theoretical loss, simply by setting appropriate values for the amplitude-coupling coefficients of the optical couplers that constitute the circuit. However, a problem arises when introducing conventional optical interferometer circuits into such systems, in that the transmission spectra are theoretically periodic against optical frequency so the transmission characteristics cannot be made periodic with respect to wavelength. Therefore, if we are to use conventional optical interferometer circuits in the CWDM system, we must mitigate the walkoff of the transmission passbands from the CWDM wavelength grid.

For the purpose of realizing an interferometer circuit that can be implemented in wavelength-based optical systems, we have already proposed a novel method that can convert a frequency filter into a wavelength filter whose filter response is periodic in terms of wavelength [12]. The method uses a phase-generating coupler (PGC), which has the ability to generate a wavelength-dependent phase that converts conventional optical frequency filters into wavelength filters. We have applied this transformation method to an MZI and demonstrated an MZI with a uniform wavelength period of 40 nm.

In this paper, we detail the fundamental principle of an optical interferometer circuit with a uniform wavelength spacing. Additionally, we focus on the fabrication tolerance of a PGC and evaluate the transmission characteristics of an MZI, considering fabrication variations. In Section II, we explain the fundamental operating principle of our novel optical interferometer circuit. In Section III, we describe the use of a two-port lattice-form filter, which is an example structure of a PGC. In Section IV, we use our transformation method to convert a conventional MZI into a uniform-wavelength-spaced MZI. We optimize the PGC variables to obtain a 20-nm-channel-spaced MZI for application to CWDM systems whose channel arrangement is constant with respect to wavelength. Section V describes the fabrication of the designed MZI on a 1.5%-Δ silica-based waveguide using conventional planar lightwave circuit (PLC) fabrication technology. We demonstrate the successful fabrication of an MZI, where the wavelength displacement of the transmission peak passband from the 20-nm wavelength grid is less than $\pm 1.2\%$ of the wavelength period, regardless of polarization. Finally, we discuss the fabrication tolerance of the designed MZI in relation to fabrication variations of the PGC variables in Section VI. Section VII concludes this paper with a summary.

Manuscript received December 26, 2005; revised March 20, 2006.

The authors are with NTT Photonics Laboratories, NTT Corporation, Atsugi 243-0198, Japan (e-mail: mizuno@aecl.ntt.co.jp).

Digital Object Identifier 10.1109/JLT.2006.876342

II. Operating Principle

A. Fundamental Concept

We first describe the fundamental concept of our method for transforming a conventional optical interferometer circuit into an optical wavelength filter whose channel allocation is equally spaced with respect to wavelength. We show that by providing the delay part with a nonlinear wavelength-dependent phase generated by the PGC, we can artificially modify the path-length difference of the delay part such that the wavelength spacing is kept constant at any wavelength. We also derive the phase required to realize an MZI with a uniform wavelength period.

Fig. 1(a) shows the structure of a conventional MZI, which is one of the simplest examples of an optical interferometer circuit. The path-length difference of the upper and lower delay lines of the delay part is set at ΔL. An optical signal passing through the MZI is divided into odd and even channels, and they are alternately launched from output ports 1 and 2, respectively. The transmission spectra launched from the two output ports are characterized by periodic functions of frequency, whose frequency period Δf is determined by ΔL as

$$\Delta f = c \cdot (n_g \Delta L)^{-1} \tag{1}$$

where c is the light velocity in a vacuum, and n_g is the group refractive index. Because the optical frequency f and the wavelength λ are related to c with the equation $\lambda = c/f$, the transmission spectra of a conventional optical interferometer circuit that is periodic with respect to frequency is, in principle, not periodic with respect to wavelength. This is directly revealed by the transmission spectra of the optical filter. If we assume that the peak wavelengths of the ith and $(i+2)$th transmission bands launched from one of the output ports of the MZI are λ_i and λ_{i+2}, respectively, the wavelength period of the two transmission bands is given by

$$\Delta\lambda_{i,i+2} = \lambda_i \cdot \lambda_{i+2} (n_g \Delta L)^{-1} \tag{2}$$

where $\Delta\lambda_{i,i+2} = \lambda_{i+2} - \lambda_i$. Because the path-length difference ΔL is a constant value, it is confirmed from (2) that the wavelength spacing changes according to the wavelength. Thus, the transmission spectrum of a conventional MZI is obviously not periodic with respect to wavelength.

Fig. 1(b) shows the transmission spectra of a conventional MZI, where ΔL is set so that the wavelength period becomes approximately 40 nm at a center wavelength of $\lambda_c = \lambda_5 = 1550$ nm. The CWDM wavelength grid in Fig. 1(b) is equally allocated with a 20-nm separation in the range of 1470–1610 nm. The peak wavelengths of the transmission bands correspond to the wavelength grid at 1530 and 1550 nm. This is because the wavelength period is approximately 40 nm at the center wavelength. However, at other wavelengths, the peak wavelengths are displaced from the CWDM grid because the wavelength period changes with wavelength. This wavelength displacement becomes larger when the wavelength region is further from the center. For example, the wavelength displacement becomes as large as 10% and 5% of the wavelength period of 40 nm at both ends of the wavelength grid of 1470 and 1610 nm, respectively.

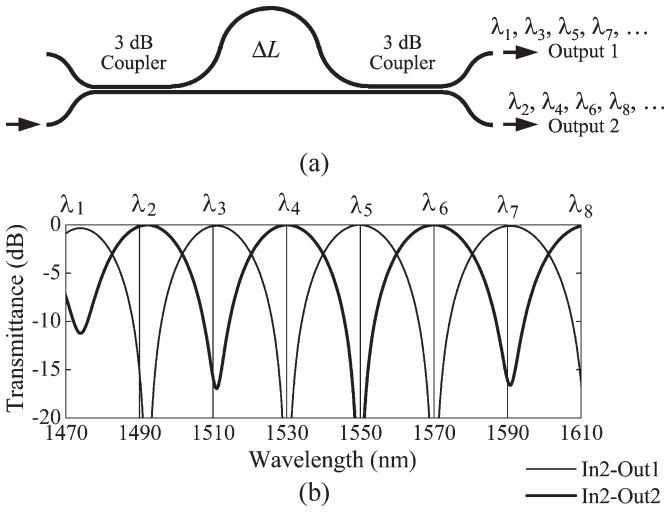

Fig. 1. (a) Schematic diagram and (b) calculated transmission spectra of a conventional MZI. The path-length difference ΔL of the MZI delay part is set so that the wavelength period becomes approximately 40 nm at a center wavelength of 1550 nm.

If the wavelength spacing $\Delta\lambda_{i,i+2}$ in (2) can be kept constant regardless of the transmission wavelength, the wavelength spacing of the MZI will become uniform. We have already found that this can be accomplished by providing the MZI delay part with an appropriate amount of wavelength-dependent phase generated by a PGC. Usually, the phase difference between the lights launched from the two output ports of a conventional optical coupler is constant. In contrast, the PGC can generate an arbitrary wavelength dependence in the phase of the light launched from its output ports. At the same time, the PGC functions as a coupling element with an arbitrary wavelength dependence. We provide a detailed theoretical description of a PGC in Section III.

The path-length difference ΔL of a conventional MZI is a fixed value. However, using the phase created by the PGC, ΔL can artificially be made wavelength dependent. Such an effective path-length difference $\Delta\widetilde{L}$ is given by

$$\Delta\widetilde{L} = \Delta L - \Theta\lambda \cdot n_c^{-1} \tag{3}$$

where Θ is a phase of the light launched from the output ports of the PGC, and n_c is the effective refractive index of a waveguide. By providing an appropriate phase Θ so that $\Delta\lambda_{i,i+2}$ becomes constant at any wavelength, we can realize an MZI with a uniform wavelength period. Substituting ΔL in (2) with the effective path-length difference $\Delta\widetilde{L}$ in (3) produces a relational expression for the phase Θ_{i+1} and wavelength λ_{i+1} of the $(i+1)$th transmission band:

$$(\lambda_{i+2} - \lambda_i)\left(\Delta L - \Theta_{i+1}\lambda_{i+1} \cdot n_c^{-1}\right) = \lambda_i \cdot \lambda_{i+2} \cdot n_g^{-1}. \tag{4}$$

By arranging (4), the phase output from the PGC Θ_{i+1} is expressed as a function of wavelength

$$\Theta_{i+1} = \frac{n_c}{\lambda_{i+1}}\left[\Delta L - \frac{1}{n_g} \cdot \left(\frac{1}{\lambda_i} - \frac{1}{\lambda_{i+2}}\right)^{-1}\right]. \tag{5}$$

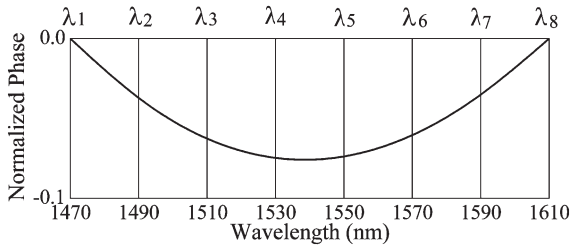

Fig. 2. Nonlinear phase needed to realize an MZI with a uniform wavelength period of 40 nm. The phase is directly related to the displacement of the center of the MZI transmission passbands from the 20-nm-spaced CWDM grid.

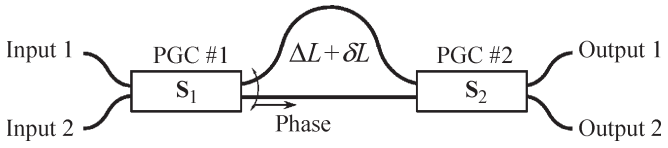

Fig. 3. Schematic diagram of a novel MZI where conventional directional couplers are each replaced with a PGC.

Because the ith and $(i+2)$th transmission bands are one channel spacing (equal to half the wavelength period) smaller and larger than the $(i+1)$th transmission band, respectively, λ_i and λ_{i+2} are each related to λ_{i+1} as $\lambda_i = \lambda_{i+1} - \Delta\lambda/2$ and $\lambda_{i+2} = \lambda_{i+1} + \Delta\lambda/2$. Using these two equations, we derive the following approximation:

$$\left(\frac{1}{\lambda_i} - \frac{1}{\lambda_{i+2}}\right)^{-1} \cong \frac{\Delta\lambda}{\lambda_{i+1}^2}. \tag{6}$$

By using (6) and replacing λ_{i+1} with λ, we obtain the phase Θ required to transform a conventional MZI into an MZI whose transmission spectra is periodic with respect to wavelength

$$\Theta = \frac{n_c \cdot \Delta L}{\lambda} - \frac{\lambda \cdot n_c}{n_g \cdot \Delta\lambda}. \tag{7}$$

Fig. 2 shows the nonlinear part of the phase Θ needed to realize an MZI with a uniform wavelength period of 40 nm. A comparison with the transmission spectra in Fig. 1(b) shows that the phase required to produce the novel MZI is directly related to the displacement of the center of the transmission bands from the 20-nm-spaced CWDM grid. For example, we would require a phase of 0.2 rad to mitigate a wavelength displacement of 1 nm.

B. Required Phase

As explained previously, a nonlinear wavelength-dependent phase can be created by using the PGC. Fig. 3 shows the schematic diagram of the proposed MZI, where two optical couplers are replaced with PGCs. The wavelength response of such a filter is given by

$$X(\lambda) = \sum_{q=0}^{N} x_q \exp\left\{-j2\pi q\left[\frac{n_c \Delta L'}{\lambda} - \Psi(\lambda)\right]\right\} \tag{8}$$

where x_q is the amplitude coefficient, $\Delta L'$ is the path-length difference of the optical delay part of the proposed MZI, and $\Psi(\lambda)$ is the phase generated by the two PGCs. To realize an

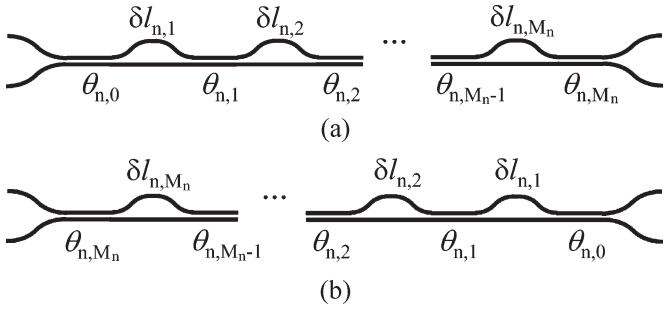

Fig. 4. (a) Schematic diagram of a two-port lattice-form PGC. (b) Schematic diagram of a PGC with the same structure as that in (a) but flipped horizontally. The amplitude-coupling ratios of the PGCs are the same, but the phases generated by these two PGCs are different.

MZI whose transmission characteristics are a periodic function of wavelength, a nonlinear phase is needed as described by the following equation:

$$\Psi(\lambda) = n_c(\Delta L + \delta L)\cdot\lambda^{-1} + \Delta\lambda^{-1}\cdot\lambda - (m + \lambda_c\Delta\lambda^{-1}) \tag{9}$$

where δL is the additional minute path-length difference of the delay part, $\Delta\lambda$ is the wavelength period (equal to twice the channel spacing), m is an integer, and λ_c is the center wavelength. This equation is composed of three terms, namely 1) nonlinear part; 2) linear part; and 3) constant. By expanding (9), the required phase is approximated by a polynomial expression of wavelength

$$\Psi(\lambda) \cong \sum_q A_q(\lambda - \lambda_c)^q \tag{10}$$

where A_q is the expansion coefficient given by

$$A_0 = n_{\rm co}\Delta L'\lambda_c^{-1} - m \tag{11}$$

$$A_1 = \frac{-n_{\rm co}\Delta L'}{\lambda_c^2} + \frac{\Delta L'}{\lambda_c}\cdot\left.\frac{dn_c}{d\lambda}\right|_{\lambda=\lambda_c} + \frac{1}{\Delta\lambda} \tag{12}$$

$$A_q = \frac{(-1)^q\Delta L'}{\lambda_c^q}\left(\frac{n_{\rm co}}{\lambda_c} - \left.\frac{dn_c}{d\lambda}\right|_{\lambda=\lambda_c}\right) \quad (\text{when } q \geq 2). \tag{13}$$

Here, $n_{\rm co}$ is the effective refractive index of a waveguide at center wavelength λ_c, and the second derivative of n_c is approximated as 0.

In the following section, we describe the fundamental structure and theory of a PGC that can generate a nonlinear wavelength-dependent phase and simultaneously function as an optical coupler.

III. PGC

A. Two-Port Lattice-Form PGC

There are many ways of realizing a PGC. Of the numerous methods, we used a two-port lattice-form filter composed of $M+1$ optical couplers and M optical delay lines as a PGC (Fig. 4). Furthermore, we used a directional coupler as an optical coupler. We used this filter structure to form the PGC because it is theoretically lossless. Moreover, we found that by optimizing the effective optical path-length differences of the delay parts and the amplitude-coupling ratios of the

directional couplers, the PGC can generate an arbitrary nonlinear wavelength-dependent phase and, at the same time, function as an optical coupler.

In this section, we derive the basic equations of a two-port lattice-form PGC. The transfer matrix of an nth two-port lattice-form PGC is given by the following 2×2 unitary matrix:

$$\mathbf{S}_n = \begin{bmatrix} H_n(z) & -F_{n^*}(z) \\ F_n(z) & H_{n^*}(z) \end{bmatrix} \tag{14}$$

where $H_n(z)$ and $F_n(z)$ indicate the through-port and cross-port transfer functions, respectively, and $z_{n,p}$ is a complex variable equal to $\exp(j2\pi\delta l_{n,p}/\lambda)$. The subscript $*$ represents a para-Hermitian conjugate, where $H_{n^*}(z)$ is defined as

$$H_{n^*}(z) = H_n^*\left(\frac{1}{z^*}\right) \tag{15}$$

with the superscript $*$ indicating the ordinary complex conjugate [13]. The transfer matrix $\mathbf{S}_n$ is a unitary matrix that satisfies the paraunitary property defined as $\mathbf{S}_n(z) \cdot \mathbf{S}_{n^*}(z) = \mathbf{E}$, where $\mathbf{E}$ is an identity matrix. Therefore, $\mathbf{S}_{n^*}$ is a para-Hermitian conjugate matrix of $\mathbf{S}_n$ written as follows:

$$\mathbf{S}_{n^*} = \mathbf{S}_n^{-1} = \begin{bmatrix} H_{n^*}(z) & F_{n^*}(z) \\ -F_n(z) & H_n(z) \end{bmatrix}. \tag{16}$$

Moreover, the transfer matrices of the two-port lattice-form PGCs are defined so that they satisfy the unimodulus condition defined as

$$H_n(z)H_{n^*}(z) + F_n(z)F_{n^*}(z) = 1 \tag{17}$$

for the transfer matrix $\mathbf{S}_n$. The total transfer matrix is disassembled into unit element transfer matrices: a first directional coupler and M_n unit cells connected to the first directional coupler, where each unit cell comprises a directional coupler and an optical delay part. The transfer matrix of the first directional coupler is

$$\mathbf{S}_{n,0} = \begin{pmatrix} \cos\theta_{n,0} & -j\sin\theta_{n,0} \\ -j\sin\theta_{n,0} & \cos\theta_{n,0} \end{pmatrix} \tag{18}$$

and the transfer matrix of the pth unit cell is

$$\mathbf{S}_{n,p} = \begin{pmatrix} \cos\theta_{n,p}{z_{n,p}}^{-1/2} & -j\sin\theta_{n,p}{z_{n,p}}^{-1/2} \\ -j\sin\theta_{n,p}{z_{n,p}}^{1/2} & \cos\theta_{n,p}{z_{n,p}}^{1/2} \end{pmatrix} \tag{19}$$

where $z_{n,p}$ is equal to $\exp(j2\pi\delta l_{n,p}/\lambda)$, $\delta l_{n,p}$ is the effective optical path-length difference of the pth optical delay part, which includes an effective refractive index, and $\theta_{n,p}$ is the angular expression of the wavelength-dependent amplitude-coupling ratio of the pth optical coupler of the nth PGC. Using the transfer matrix of the directional coupler and the unit cells in (18) and (19), the transfer matrix $\mathbf{S}_n$ is summed up as

$$\mathbf{S}_n = \prod_{p=M_n}^{0} \mathbf{S}_{n,p}. \tag{20}$$

B. Two-Port Lattice-Form PGC With Mirror-Symmetric Structure

Fig. 4(b) shows the structure of a two-port lattice-form PGC that has the same structure as that in Fig. 4(a) but flipped horizontally. The transfer matrix $\widetilde{\mathbf{S}}_n$ of this mirror-symmetric PGC is also given by a 2×2 unitary matrix, where $\widetilde{\mathbf{S}}_n$ is related to the transfer matrix $\mathbf{S}_n$ in (20) by

$$\widetilde{\mathbf{S}}_n = \prod_{p=0}^{M_n} \mathbf{S}_{n,p}^{\mathrm{T}} = \left(\prod_{p=M_n}^{0} \mathbf{S}_{n,p}\right)^{\mathrm{T}} = \mathbf{S}_n^{\mathrm{T}}. \tag{21}$$

The amplitude-coupling ratios of the PGCs in Fig. 4(a) and (b) are the same, but the phases generated by these two PGCs are different.

IV. MZI Design

A. Phase Design

The phase generated by the PGCs is the difference between the phases of the lights launched from the two output ports of the PGC. When there are two PGCs, their overall phase depends on the MZI ports in use. For example, if light is launched into input port 2, the through-port phase $\Phi^{(t)}(\lambda)$ is written as

$$\Phi^{(t)}(\lambda) = \{\arg[-F_{1^*}(z)] + \arg[F_2(z)] - \arg[H_{1^*}(z)] - \arg[H_{2^*}(z)]\}/2\pi \tag{22}$$

and the cross-port phase $\Phi^{(c)}(\lambda)$ is written as

$$\Phi^{(c)}(\lambda) = \{\arg[-F_{1^*}(z)] + \arg[H_2(z)] - \arg[H_{1^*}(z)] - \arg[-F_{2*}(z)]\}/2\pi \tag{23}$$

by using the transfer functions in (14), where $\arg(z)$ is the complex argument of z. Modifying (23) and comparing it with (22), we obtain the following relationship between $\Phi^{(t)}(\lambda)$ and $\Phi^{(c)}(\lambda)$:

$$\Phi^{(c)}(\lambda) = \Phi^{(t)}(\lambda) - (m' - 1/2) \tag{24}$$

where m' is an integer. The components of the phase Φ are summarized by using the through-port phase $\Phi(\lambda)(= \Phi^t(\lambda))$ as

$$\mathbf{\Phi} = \begin{bmatrix} \Phi(\lambda) - m'_{11} & \Phi(\lambda) - (m'_{21} - 1/2) \\ \Phi(\lambda) - (m'_{12} - 1/2) & \Phi(\lambda) \end{bmatrix}. \tag{25}$$

The through-port phase needed to realize an MZI whose transmission characteristics are a periodic function of wavelength is given as

$$\Psi_t(\lambda) = n_c(\Delta L + \delta L)\cdot\lambda^{-1} + \Delta\lambda^{-1}\cdot\lambda - \left(m\cdot 2^{-1} + \lambda_c^{(t)}\Delta\lambda^{-1}\right). \tag{26}$$

This function is almost the same as that in (9); the only difference being that $m/2$ is used instead of m. In this way, we can choose whether the transmission spectrum at the center wavelength λ_c is a passband with maximum transmittance (when m is even) or a rejection band with minimum transmittance (when m is odd). In other words, we can choose to launch the light

with wavelength λ_c from the through-port when m is even or from the cross-port when m is odd. On the other hand, if we use m as is the case with (9), the light with wavelength λ_c is always launched from the through-port.

The transmission characteristics of the through-port and the cross-ports are shifted away from each other by half the wavelength spacing, that is, $\lambda_c^{(c)} = \lambda_c^{(t)} \pm \Delta\lambda/2$. Therefore, the desired phase for the cross-port is related to $\Psi_t(\lambda)$ by

$$\Psi_c(\lambda) = \Psi_t(\lambda) \mp 1/2. \tag{27}$$

As noticed from (25), the phase generated by the PGC differs, depending on which input and output ports of the MZI are used. However, the relation in (27) implies that we only need to optimize either the through-port phase $\Psi_t(\lambda)$ or the cross-port phase $\Psi_c(\lambda)$.

B. Optimization of PGC Design Parameters

When performing the numerical calculation, we imposed several constraints on the PGC design variables to simplify the optimization and to improve the fabrication tolerance of the novel MZI. We used identical PGCs for the two couplers and placed them symmetrically around the center of the MZI delay part. More specifically, we used the structures in Fig. 4(a) and (b) for the first and second couplers, respectively. In this way, the phases of the lights launched from the two PGCs are combined. With this restriction and using $-F_{1*}(z) = F_2(z) = -F_*(z)$ and $H_{1^*}(z) = H_{2^*}(z) = H_*(z)$ derived from the relation $S_2 = \widetilde{S}_1 = S_1^{\mathrm{T}}$, we can simplify (22) into

$$\Phi(\lambda) = \{\arg[-F_*(z)] - \arg[H_*(z)]\}/\pi. \tag{28}$$

Additionally, we set the amplitude-coupling ratios of all the directional couplers at the same variable $\theta(\lambda)$ and set $\delta l_1 + \delta l_3 = 0$.

We used the conjugate gradient method to optimize the PGC variables. The conditions for optimum MZI design are summarized in Appendix. As a result of optimization, we found that a three-stage lattice-form structure is sufficient to realize a PGC with a good degree of approximation. The PGC variables obtained by the optimization are $\theta(\lambda_c) = 0.42$, $\delta l_1 = 1.7\ \lambda_c$, $\delta l_2 = 0.3\ \lambda_c$, $\delta l_3 = -1.7\ \lambda_c$, and $\delta L = 0.1\ \lambda_c$. Fig. 5 shows the wavelength dependence of the amplitude-coupling ratio and the phase generated by the designed PGC. The phase generated by the PGC is approximated by the following third-order polynomial:

$$\begin{aligned}\Psi^{(t)}(\lambda) &\cong \sum_{q=0}^{3} y_q(\lambda - \lambda_c)^q \\ &= 0.60 + 0.42 \cdot (\lambda - \lambda_c) \\ &\quad + 16 \cdot (\lambda - \lambda_c)^2 - 10 \cdot (\lambda - \lambda_c)^3.\end{aligned} \tag{29}$$

Both figures suggest that we obtained good design parameters with the PGC phase and amplitude-coupling ratio close to the desired characteristics. If we were to impose no optimization restrictions, there would be more flexibility in the PGC design. A lattice-form filter with smaller filter stages may be sufficient to realize a PGC with the desired characteristics. However, when we consider ease of fabrication, imposing the preceding restrictions is reasonable. Moreover, even with these restrictions, the PGC variables that we obtained showed a good degree of approximation, with which the PGC generates the desired phase and simultaneously functions as a wavelength-independent 3-dB coupler.

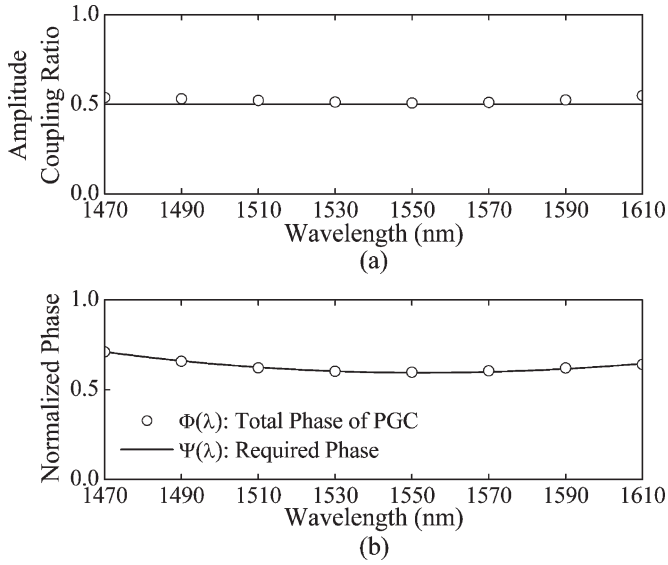

Fig. 5. Calculated wavelength dependence of (a) amplitude-coupling ratio and (b) phase of the optimized PGC. These figures suggest that we obtained good PGC design parameters close to the desired characteristics.

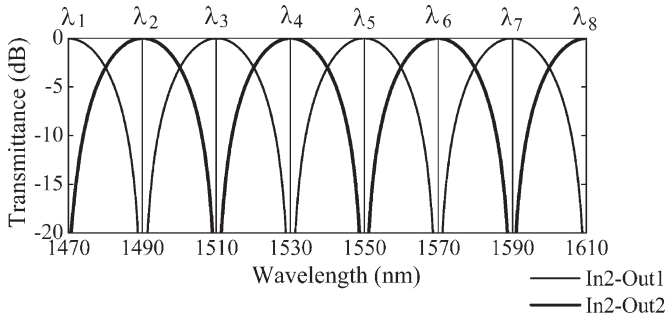

Fig. 6. Calculated transmission spectra of a 20-nm-spaced MZI incorporating the designed PGC. The peak wavelengths λ_1 through λ_8 match the CWDM wavelength grid because the channel spacing is exactly uniform with respect to wavelength. Moreover, the extinction ratio is excellent because of the small wavelength dependence of the amplitude-coupling ratio of the PGC.

C. Calculation of Transmission Spectra

Fig. 6 shows the calculated transmission spectra of the novel MZI. Because the channel spacing is exactly uniform with respect to wavelength, the peak wavelengths of the transmission passbands match the CWDM wavelength grid. In contrast, the wavelength spacing of the transmission passbands of a conventional MZI is theoretically not uniform with respect to wavelength, as shown in Fig. 1(b). Moreover, the capability of the PGC to function as a wavelength-independent coupler is another advantage over conventional optical couplers. The extinction ratio of the novel MZI is excellent throughout the whole wavelength region because of the small wavelength dependence

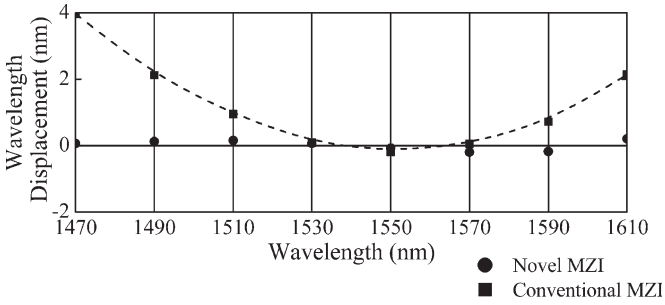

Fig. 7. Calculated wavelength displacement between the centers of the transmission passbands from the CWDM wavelength grid of the conventional and novel MZIs. The wavelength displacement of the novel MZI is only one-fifth that of a conventional MZI.

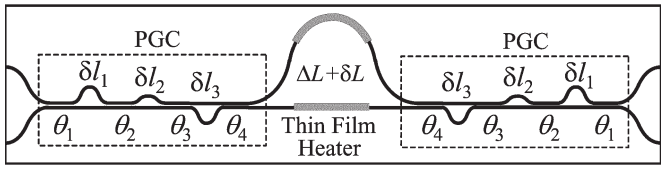

Fig. 8. Schematic diagram of the novel MZI fabricated with a 1.5%-Δ silica-based waveguide. Thin-film heaters were formed on the MZI delay part, and a permanent heat treatment technique was used to mitigate both the path length error and the waveguide birefringence.

of the amplitude-coupling ratio of the PGCs. In comparison, the extinction ratio of a conventional MZI deteriorates at certain wavelengths, as shown in Fig. 1(b), because of the wavelength dependence of conventional optical couplers.

Fig. 7 shows the calculated wavelength displacement between the centers of the transmission passbands from the CWDM wavelength grid of the MZIs. There is no displacement at the center wavelength of 1550 nm for either MZI, but displacement occurs with the conventional MZI and it becomes larger as the wavelength moves further away from the center wavelength. The maximum wavelength displacement of a conventional MZI within the wavelength range of 1490–1590 nm is ± 2 nm at 1490 nm, which is approximately $\pm 5\%$ that of the wavelength period of 40 nm. On the other hand, we can maintain the wavelength displacement at less than ± 0.4 nm ($\pm 1\%$ of the wavelength period of 40 nm), which is only one-fifth that of a conventional MZI.

V. Experimental Results

A. Fabrication

The designed MZIs were fabricated with conventional GeO_2-doped silica-based PLC fabrication technology, which consists of flame hydrolysis deposition, photolithography, and reactive ion etching [14]. After patterning the waveguide, thin-film heaters were formed on the delay part, as shown in Fig. 8. A waveguide with a high refractive index difference of 1.5% is used to reduce the minimum bending radius to 2 mm. The core cross section is 4.5×4.5 μm^2, and the chip size is 35×5 mm^2. Previously reported spot-size converters were integrated into both the input and output ports of the MZI [15]. The spot-size converters reduced the large single-mode fiber coupling loss of the 1.5%-Δ waveguides from 1.8 to 0.4 dB at a single waveguide junction.

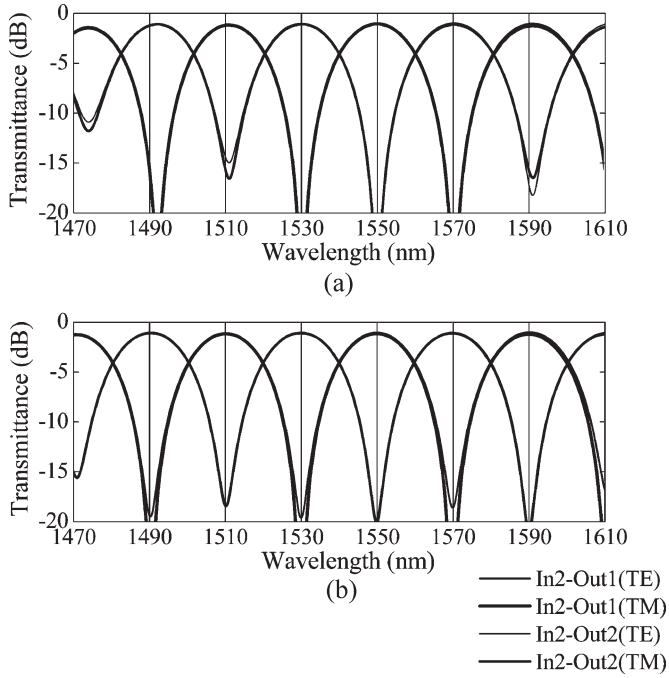

Fig. 9. Measured transmission spectra of (a) conventional MZI (b) novel MZI.

B. Birefringence and Path Length Adjustment

When there are variations in the refractive index caused by fabrication errors, the optical path length changes, which results in a center wavelength shift. Moreover, the difference between the thermal expansion coefficients of a silicon substrate and a silica-based waveguide causes waveguide birefringence related to asymmetric compressive stress. This waveguide birefringence causes a polarization-dependent wavelength shift. These effects can change the characteristics of the PGC and the MZI delay part.

The effect of the optical path length error and the waveguide birefringence becomes larger as the path-length difference increases. The path-length difference of the MZIs used in the CWDM systems is much smaller than that of the MZIs used in the DWDM systems. Therefore, we rarely have to consider the effect of the optical path length changes and the waveguide birefringence. However, to acquire an MZI with the best characteristics, we have used a permanent heater trimming technique that can control both the path length error and waveguide birefringence [16]. Because the path-length differences of the PGC delay parts are only of wavelength order, the effect of the optical path length changes and the waveguide birefringence are negligible. Thus, we have only applied this technique to the MZI delay part to adjust $n_c \Delta L'$ in (8).

C. Measurement of Transmission Spectra

We measured the transmission spectra of the fabricated MZIs using an optical spectrum analyzer and the amplified spontaneous emission from an Er-doped fiber. Fig. 9 shows the measured transmission spectra of the conventional and novel MZIs.

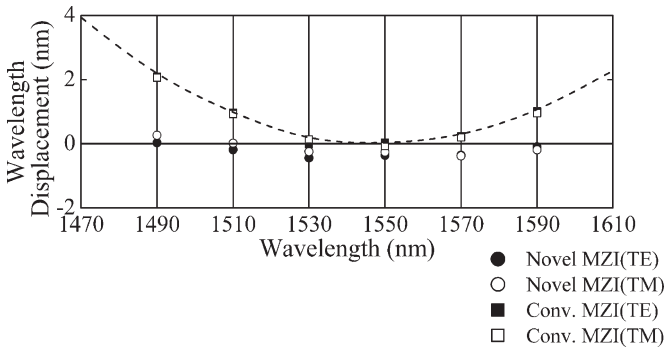

Fig. 10. Measured wavelength displacement of the conventional and novel MZIs.

The peak wavelength of the transmission passband of the conventional MZI is aligned at the center wavelength of 1550 nm. However, with other wavelength grids, there is wavelength displacement, which becomes larger as the wavelength moves away from the center. On the other hand, the peak wavelength of the transmission passband of the novel MZI is exactly aligned with the CWDM wavelength grid because the transmission spectra are equally spaced with respect to wavelength. Fig. 10 shows the experimental wavelength displacement against the CWDM wavelength grid for both MZIs. The maximum wavelength displacement of the conventional MZI is ± 2 nm ($\pm 5\%$ of the wavelength period of 40 nm) at 1490 nm, whereas the displacement of the novel MZI is less than ± 0.5 nm ($\pm 1.2\%$ of the wavelength period) from 1490 to 1590 nm, regardless of polarization. The polarization-dependent wavelength shift is less than 0.2 nm, which is only 0.5% of the wavelength period. We thus confirmed that we successfully converted a conventional MZI that is theoretically periodic with respect to frequency into an MZI with a uniform wavelength period.

Because the channel spacing of the novel MZI is exactly the same as the CWDM grid spacing, we have improved the insertion loss and crosstalk on the CWDM grid. The maximum CWDM grid insertion loss within the wavelength range of 1490–1590 nm of the novel MZI was 1.2 dB including a single-mode fiber coupling loss of 0.4 dB $\times$ 2, a propagation loss of 0.2 dB, and an excess loss of 0.2 dB. This value was 0.6 dB smaller than that of the conventional MZI. The minimum CWDM grid crosstalk in the 1490–1590-nm wavelength range was -17 dB, which was 4 dB better than that of the conventional MZI.

VI. Discussion

In this section, we discuss the fabrication tolerance of a lattice-form PGC. The optimum PGC design parameters change according to the allowable degree of approximation or the restrictions imposed on the design variables. Theoretically, the best design parameter is the one that produces the best degree of approximation. However, in terms of mass production, it is important to consider the fabrication tolerance with regard to the PGC designs.

In Section IV, we imposed several restrictions on the three-stage lattice-form PGC. They include setting the amplitude-coupling ratio of all the couplers at the same value and setting the path-length difference of the first and third delay parts at $\delta l_1 + \delta l_3 = 0$. The former restriction was incorporated in the PGC design specifically to facilitate the fabrication of the individual coupler that constitutes the PGC. The latter restriction increases the symmetry of the PGC delay part. To examine the effectiveness of these restrictions, we compare the theoretical and experimental characteristics of the following three types of MZI:

1) a novel MZI with high PGC symmetry (the same design as that described in Sections IV and V);
2) a novel MZI with low PGC symmetry that uses the same amplitude-coupling ratios for all the couplers but where there is no constraint as regards the delay part;
3) a conventional MZI.

The PGC used for the first type of MZI was described in Sections IV and V. The PGC used for the second type of MZI was designed using the procedure described in Section IV. The PGC design parameters for the second type of MZI obtained by the optimization are $\theta(\lambda_c) = 0.49$, $\delta l_1 = 0.2\ \lambda_c$, $\delta l_2 = 0.3\ \lambda_c$, $\delta l_3 = -2.3\ \lambda_c$, and $\delta L = -1.1\ \lambda_c$. Because this PGC has low symmetry but a large degree of freedom, the amplitude-coupling ratio and the phase generated by this PGC are closer to the desired characteristics than the first PGC design with stricter constraints. For example, the amplitude-coupling ratios of the first and second PGC designs are $50\% \pm 4\%$ and $50\% \pm 2\%$, respectively, and the maximum error between the required phase and the phase of the PGC with the first and second designs are 0.6% and 0.5%, respectively, within the 1470–1610-nm wavelength range (note that the amplitude-coupling ratio of the conventional 3-dB coupler is $50\% \pm 10\%$, and the maximum wavelength displacement of the conventional MZI converted into phase is 10% in the 1470–1610-nm wavelength range). Because the second PGC has more flexibility with respect to the PGC design variables, both the amplitude-coupling ratio and the phase of the PGC are closer to the desired characteristics.

The fabrication error of the amplitude-coupling angle of the individual couplers that constitute the PGCs changes the characteristics of the novel MZIs. To evaluate the effect of coupling angle variation on the MZI characteristics, we simulated and fabricated several MZIs, including some with no amplitude-coupling ratio error and some with smaller and larger amplitude-coupling ratios than the optimum value. In this simulation and experiment, we assumed that all four of the individual couplers that constitute the PGCs have the same amplitude-coupling ratio. From the calculated and measured transmission spectra, we obtained the peak wavelengths of each transmission passband of the MZIs. Fig. 11 shows the theoretical and experimental wavelength displacement of the passband peak wavelengths from the CWDM wavelength grid. Fig. 11(a) shows the results for the novel MZI with high PGC symmetry. The amplitude-coupling ratio variation of the individual couplers that constitute the PGC is set at -0.03, 0 (no fabrication error), and 0.03. More specifically, when the amplitude-coupling ratio of all four of the individual couplers that constitute the PGC is $\theta = 0.42$, as shown in Fig. 8, the amplitude-coupling ratio variations of -0.03, 0, and 0.03

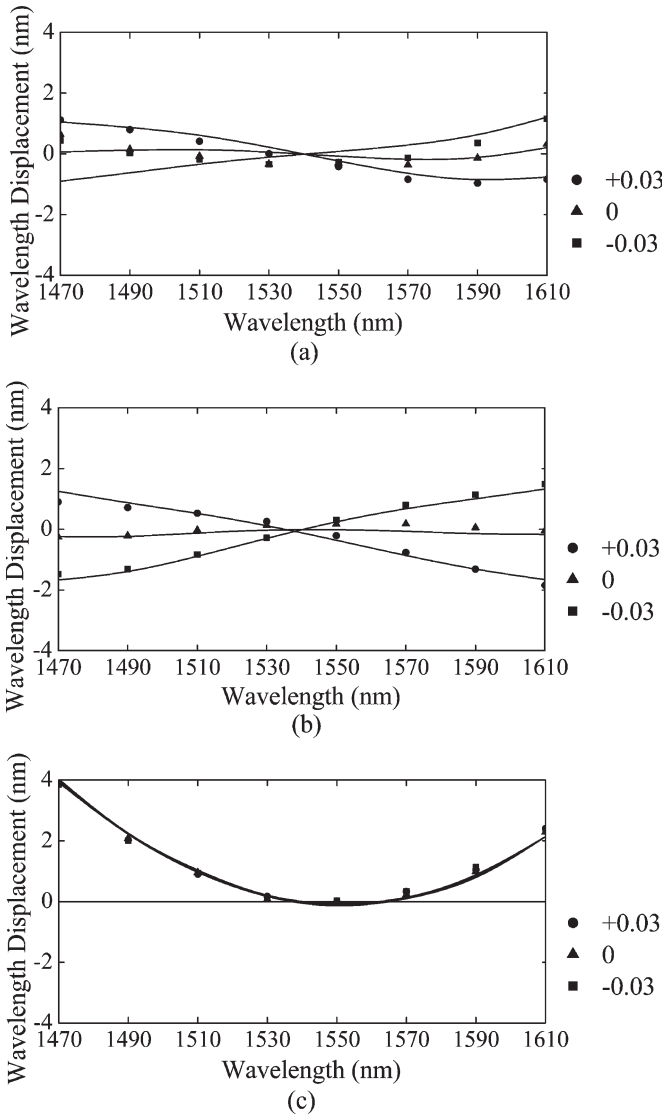

Fig. 11. Calculated and measured wavelength displacement of the transmission passband peak wavelengths from the CWDM grid. (a) Novel MZI with high PGC symmetry. (b) Novel MZI with low PGC symmetry. (c) Conventional MZI. The amplitude-coupling angle variation of the directional couplers is set at $+0.03$, 0 (no fabrication error), and -0.03. Dot: measurement. Line: calculation.

correspond to the amplitude-coupling ratios of $\theta = 0.39$, 0.42, and 0.45, respectively. The wavelength displacement changes depending on the variations in the amplitude-coupling ratio. This implies that the phase generated by the PGC deviates from the required phase when the couplers that constitute the PGC suffer from fabrication error. The maximum wavelength displacement of this first type of MZI with high PGC symmetry is ± 1 nm ($\pm 2.5\%$ of the wavelength period) when there is an amplitude-coupling ratio error of 0.03. Fig. 11(b) shows the results for a novel MZI with low PGC symmetry. The novel MZI with low PGC symmetry is more sensitive than the novel MZI with high PGC symmetry to fabrication variations in the individual couplers of the PGC. The wavelength displacement of this MZI becomes ± 1.5 nm at an amplitude-coupling ratio error of -0.03. In contrast to the novel MZIs, the wavelength displacement of a conventional MZI remains the same regardless of the amplitude-coupling ratio error [Fig. 11(c)]. These features prove theoretically and experimentally that the phase generated by the PGC virtually acts as a wavelength-dependent delay part that can control the wavelength spacing of an MZI.

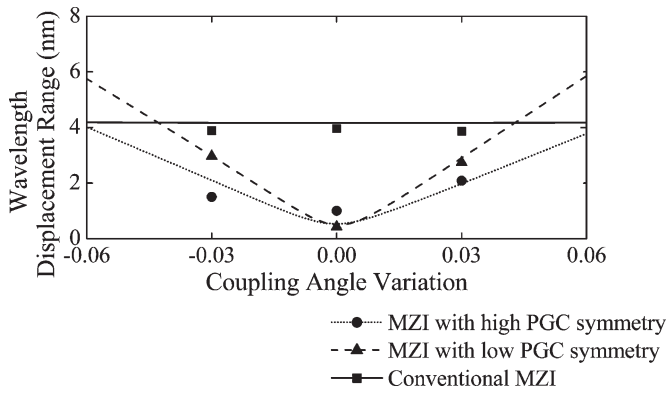

Fig. 12. Fluctuation range of the wavelength displacement against the coupling angle variation of the directional couplers that constitute the PGC. The wavelength displacement range is the difference between the maximum and minimum wavelength displacement in the 1470–1610-nm wavelength range. Dot: measurement. Line: calculation.

The fact that the PGC with higher symmetry has a larger fabrication tolerance can also be shown in Fig. 12. This figure shows the difference between the maximum and minimum wavelength displacement in the 1470–1610-nm wavelength range (fluctuation range) against the amplitude-coupling ratio variation of the couplers that constitute the PGC. The fluctuation range of the wavelength displacement for a conventional MZI is always 4.2 nm, regardless of the fabrication variations between the couplers. These theoretical and experimental results confirm that the fabrication variations between the couplers do not affect the wavelength displacement of the conventional MZI. On the other hand, the fluctuation range of the wavelength displacement changes for the novel MZIs. This is because the effective delay part of the novel MZIs is the sum of the actual delay part and the virtual delay related to the phases of the PGCs, which changes according to fabrication variations. When there is no amplitude-coupling ratio error, the use of the PGC with lower symmetry provides the best characteristics because the degree of approximation is larger than that of the first design with more restrictions. However, the wavelength displacement increases as the amplitude-coupling ratio error becomes larger. To keep the wavelength displacement smaller than that of a conventional MZI, we would have to fabricate the individual coupler of the PGC with a fabrication variation of no more than ± 0.04. There are many reasons for the amplitude-coupling ratio variation. If we assume that the fabrication error of the individual couplers that constitute the PGCs is mainly caused by the refractive index variation, an amplitude-coupling ratio variation of ± 0.04 corresponds to a refractive index variation of approximately $\pm 0.06\%$. The allowable fabrication variation of the amplitude-coupling ratio for the novel MZI with high PGC symmetry is ± 0.06, corresponding to a refractive index variation of approximately $\pm 0.09\%$, which is 1.5 times larger than that of the PGC with low symmetry. Therefore, the first design has an advantage in terms of mass production with a large fabrication tolerance.

To summarize, the feature discussed in this section confirms that the PGC actually generates a wavelength-dependent phase because the wavelength displacement of the novel MZI changes according to fabrication variations in the individual couplers, whereas the wavelength displacement of the conventional MZI remains the same. Moreover, the difference in the PGC design affects the impact that fabrication variations have on the MZI characteristics; thus, when we design a PGC, we should take into account the fabrication tolerance as well as other criteria including the degree of approximation and the PGC size.

VII. Conclusion

We have described the fundamental operating principle of an optical interferometer whose transmission spectra are uniform with respect to wavelength. As an example, we have used our method to design a 20-nm-spacing MZI and have fabricated the circuit using silica-based PLC technology. We have successfully realized an MZI whose wavelength displacement from the 20-nm wavelength grid is less than $\pm 1.2\%$ of the wavelength period, regardless of polarization. Moreover, we have discussed MZIs with different PGC designs and shown theoretically and experimentally that a certain design can increase the fabrication tolerance.

Appendix
Conditions for Optimum Interferometer Design

The power transmission characteristics of an optical interferometer circuit incorporating PGCs is given by

$$X(\lambda)X_*(\lambda) = \sum_{q=0}^{N} y_q \cos\left\{2\pi q\left[\frac{n_c \Delta L'}{\lambda} - \Psi(\lambda)\right]\right\}. \quad (30)$$

With an MZI, the coefficients y_q can be written as a function of $|F_1|$ and $|F_2|$. When q is equal to 0, the through-port and cross-port coefficients are

$$y_0^{(t)}(F_1, F_2) = |F_1|^2 + |F_2|^2 - 2\left(|F_1| \cdot |F_2|\right)^2 \quad (31)$$

and

$$y_0^{(c)}(F_1, F_2) = 1 - |F_1|^2 - |F_2|^2 + 2\left(|F_1| \cdot |F_2|\right)^2 \quad (32)$$

respectively. When q equals 1, the through-port and cross-port coefficients are identical, and the coefficients are written as

$$\begin{aligned} y_1^{(t)}(F_1, F_2) &= y_1^{(c)}(F_1, F_2) \\ &= 2\left[\left(1 - |F_1|^2\right) \cdot \left(1 - |F_2|^2\right)\right]^{1/2} \left(|F_1| \cdot |F_2|\right). \end{aligned} \quad (33)$$

Because $|F_1|$ and $|F_2|$ are independent variables, the conditions of the PGCs required for optimum MZI design are derived by calculating

$$\nabla \mathbf{Y}_q(F_1, F_2) \equiv \left\{\frac{\partial y_q(F_1, F_2)}{\partial |F_1|}, \frac{\partial y_q(F_1, F_2)}{\partial |F_2|}\right\} = 0. \quad (34)$$

From $\nabla \mathbf{Y}_0^{(t)}(F_1, F_2) = \nabla \mathbf{Y}_0^{(c)}(F_1, F_2) = 0$, we obtain the following system of equations: $2|F_1|(1 - 2|F_2|^2) = 0$ and $2|F_2|(1 - 2|F_1|^2) = 0$. Because $0 < |F_n| < 1$, the solution to these equations is $(|F_1|, |F_2|) = (2^{-(1/2)}, 2^{-(1/2)})$, where $y_0^{(t)} = y_0^{(c)} = 2^{-1}$. From $\nabla \mathbf{Y}_1(F_1, F_2) = 0$, we obtain the following system of equations: $|F_2|(1 - 2|F_1|^2)(1 - |F_2|^2) = 0$ and $|F_1|(1 - 2|F_2|^2)(1 - |F_1|^2) = 0$. The solution to these equations is $(|F_1|, |F_2|) = (2^{-1/2}, 2^{-1/2})$, where $y_1 = 2^{-1}$. Using the unimodulus property described by (17), we summarize the condition for obtaining an optimum MZI as

$$|H_1(z)| = |H_1(z)| = |F_1(z)| = |F_2(z)| = 2^{-1/2}. \quad (35)$$

Thus, the PGC is designed by optimizing the variables so that the phase Φ becomes identical to Ψ, and at the same time, it functions as an optical coupler that satisfies the condition in (35).

Acknowledgment

The authors would like to thank Y. Hibino for his helpful support throughout this paper.

References

[1] L. F. Stokes, M. Chodorow, and H. J. Shaw, "All-single-mode fiber resonator," *Opt. Lett.*, vol. 7, no. 6, pp. 288–290, Jun. 1982.
[2] B. Moslehi, J. W. Goodman, M. Tur, and H. J. Shaw, "Fiber-optic lattice signal processing," *Proc. IEEE*, vol. 72, no. 7, pp. 909–930, Jul. 1984.
[3] K. P. Jackson, G. Xiao, and H. J. Shaw, "Coherent optical fibre delay-line processor," *Electron. Lett.*, vol. 22, no. 25, pp. 1335–1337, Dec. 1986.
[4] N. Takato, T. Kominato, A. Sugita, K. Jinguji, H. Toba, and M. Kawachi, "Silica-based integrated optic Mach–Zehnder multi/demultiplexer family with channel spacing of 0.01–250 nm," *IEEE J. Sel. Areas Commun.*, vol. 8, no. 6, pp. 1120–1127, Aug. 1990.
[5] C. Kostrzewa and K. Petermann, "Bandwidth optimization of optical add/drop multiplexers using cascaded couplers and Mach–Zehnder sections," *IEEE Photon. Technol. Lett.*, vol. 7, no. 8, pp. 902–904, Aug. 1995.
[6] C. C. Wang, "High-frequency narrow-band single-mode fiber-optic transversal filters," *J. Lightw. Technol.*, vol. LT-5, no. 1, pp. 77–81, Jan. 1987.
[7] K. Oda, N. Takato, H. Toba, and K. Nosu, "A wide-band guided-wave periodic multi/demultiplexer with a ring resonator for optical FDM transmission systems," *J. Lightw. Technol.*, vol. 6, no. 6, pp. 1016–1023, Jun. 1988.
[8] E. L. Wooten, R. L. Stone, E. W. Miles, and E. M. Bradley, "Rapidly tunable narrowband wavelength filter using LiNbO3 unbalanced Mach–Zehnder interferometers," *J. Lightw. Technol.*, vol. 14, no. 11, pp. 2530–2536, Nov. 1996.
[9] M. Kuznetsov, "Cascaded coupler Mach–Zehnder channel dropping filters for wavelength-division-multiplexed optical systems," *J. Lightw. Technol.*, vol. 12, no. 2, pp. 226–230, Feb. 1994.
[10] K. Sasayama, M. Okuno, and K. Habara, "Photonic FDM multichannel selector using coherent optical transversal filter," *J. Lightw. Technol.*, vol. 12, no. 4, pp. 664–669, Apr. 1994.
[11] M. Oguma, T. Kitoh, Y. Inoue, T. Mizuno, T. Shibata, M. Kohtoku, and Y. Hibino, "Compact and low-loss interleave filter employing lattice-form structure and silica-based waveguide," *J. Lightw. Technol.*, vol. 22, no. 3, pp. 895–902, Mar. 2004.
[12] T. Mizuno, T. Kitoh, M. Oguma, Y. Inoue, T. Shibata, and H. Takahashi, "Mach–Zehnder interferometer with a uniform wavelength period," *Opt. Lett.*, vol. 29, no. 5, pp. 454–456, Mar. 2004.
[13] K. Jinguji and M. Kawachi, "Synthesis of coherent two-port lattice-form optical delay-line circuit," *J. Lightw. Technol.*, vol. 13, no. 1, pp. 73–82, Jan. 1995.
[14] M. Kawachi, "Silica waveguides on silicon and their application to integrated-optic components," *Opt. Quantum Electron.*, vol. 22, no. 5, pp. 391–416, Sep. 1990.

[15] T. Mizuno, T. Kitoh, M. Itoh, T. Saida, T. Shibata, and Y. Hibino, "Optical spotsize converter using narrow laterally tapered waveguide for planar lightwave circuits," *J. Lightw. Technol.*, vol. 22, no. 3, pp. 833–839, Mar. 2004.

[16] T. Mizuno, M. Kohtoku, M. Oguma, Y. Hida, and Y. Inoue, "Birefringence and path length adjustment of silica-based waveguide using permanent heater trimming," *Electron. Lett.*, vol. 40, no. 6, pp. 371–372, Mar. 2004.

Takayuki Mizuno (M'03) was born in Nagoya, Japan, in 1975. He received the B.S. degree in applied physics and the M.S. degree in crystalline materials science from Nagoya University in 1998 and 2000, respectively.

In 2000, he joined NTT Photonics Laboratories, Ibaraki (now Atsugi), Japan, where he works on silica-based optical waveguide devices.

Mr. Mizuno is a member of the IEEE Lasers and Electro-Optics Society (LEOS) and the Institute of Electronics, Information, and Communication Engineers (IEICE) of Japan.

Tsutomu Kitoh (M'91) received the B.S., M.S., and Ph.D. degrees from Nagoya University, Nagoya, Japan, in 1983, 1985, and 1996, respectively, all in electronics engineering.

In 1985, he joined the Electrical Communication Laboratories, Nippon Telegraph and Telephone Corporation (NTT), Musashino, Tokyo, where he worked on LiNbO3 optical waveguide modulators. He is currently a Senior Research Engineer with NTT Photonics Laboratories, Atsugi, Japan, where he works on the design and fabrication of silica-based planar lightwave circuits.

Dr. Kitoh is a member of the Institute of Electronics, Information, and Communication Engineers (IEICE) of Japan and the Japan Society of Applied Physics.

Manabu Oguma was born in Hokkaido, Japan, on April 7, 1966. He received the B.S. and M.S. degrees from Tohoku University, Sendai, Japan, in 1989 and 1991, respectively, both in applied physics.

In 1991, he joined the Nippon Telegraph and Telephone Corporation (NTT) Opto-Electronics Laboratories, Ibaraki (now NTT Photonics Laboratories, Atsugi), Japan, where he works on optical waveguide devices.

Mr. Oguma is a member of the Institute of Electronics, Information, and Communication Engineers (IEICE) of Japan and the Japan Society of Applied Physics.

Yasuyuki Inoue (M'94) received the B.E., M.E., and Ph.D. degrees from Kyushu University, Fukuoka, Japan, in 1987, 1989, and 1998, respectively, all in electronics engineering.

He joined Nippon Telegraph and Telephone Corporation (NTT), Ibaraki, Japan, in 1989. Since then, he has worked on silica-based planar lightwave circuits (PLC). From 1998 to 1999, he joined Photonic Integration Research Inc., (PIRI), Columbus, OH, where he worked on the commercialization of silica-based PLC devices, such as arrayed-waveguide gratings and optical splitters. He is currently a Group Leader with NTT Photonics Laboratories, Atsugi, Japan.

Dr. Inoue is a member of the Institute of Electronics, Information, and Communication Engineers (IEICE) of Japan.

Tomohiro Shibata received the B.S. degree in physics, the M.E. degree in applied physics, and the Ph.D. degree in crystalline materials science from Nagoya University, Nagoya, Japan, in 1983, 1985, and 1995, respectively.

In 1985, he joined Nippon Telegraph and Telephone Corporation (NTT) Laboratories, Ibaraki, Japan, where he worked on the epitaxial growth of thin-film semiconductors utilizing electron cyclotron resonance (ECR) plasma technology. He is currently a Senior Research Engineer with NTT Photonics Laboratories, Atsugi, Japan, where he works on the fabrication of silica-based planar lightwave circuits.

Dr. Shibata is a member of the Japan Society of Applied Physics and the Institute of Electronics, Information, and Communication Engineers (IEICE) of Japan.

Hiroshi Takahashi (M'92) was born in Japan in 1963. He received the B.S. and M.S. degrees in electrical engineering from Tohoku University, Miyagi, Japan, in 1986 and 1988, respectively, and the Ph.D. degree from Tohoku University in 1997 for his research on AWGs.

In 1988, he joined the Nippon Telegraph and Telephone (NTT) Laboratories, Ibaraki, Japan, where he worked on the fabrication and design of silica-based optical waveguide devices including arrayed-waveguide grating (AWG) wavelength multiplexers and wavelength-division multiplexing transmission systems. He is currently a Research Group Leader with the NTT Photonics Laboratories, NTT Corporation, Atsugi, Japan. His current research interest is the creation of new functional optical devices based on planar lightwave circuit technology.

Dr. Takahashi is a member of the Institute of Electronics, Information, and Communication Engineers (IEICE) of Japan and the Japan Society of Applied Physics.